recordings with a resolution of ~100 μm (*24*) and has been suggested to play an important role in the modulation of synaptic circuitry involved in motivation, reward, and learning. Here we find that the activity of individual dopaminergic presynaptic terminals is modulated by neuronal activity and receptor activation. FFNs enable optical measurements of key presynaptic processes in the central nervous system, including accumulation of a vesicle transporter substrate and release by evoked activity or drugs such as amphetamine, at unprecedented spatial resolution. FFN511 is compatible with GFP-based tags, the FM1-43 endocytic marker, and other optical probes, which will allow the construction of fine-resolution maps of synaptic microcircuitry and presynaptic activity, particularly in regions such as the hippocampus and cortex where monoamine innervation can be too sparse for electrochemical recording.

References and Notes

1. W. J. Betz, G. S. Bewick, *Science* **255**, 200 (1992).
2. G. Miesenbock, D. A. De Angelis, J. E. Rothman, *Nature* **394**, 192 (1998).
3. Q. Zhang, Y. Li, R. W. Tsien, *Science* **323**, 1448 (2009).
4. V. N. Murthy, T. J. Sejnowski, C. F. Stevens, *Neuron* **18**, 599 (1997).
5. I. J. Kopin, *Annu. Rev. Pharmacol.* **8**, 377 (1968).
6. A. Merickel, P. Rosandich, D. Peter, R. H. Edwards, *J. Biol. Chem.* **270**, 25798 (1995).
7. J. S. Partilla *et al.*, *J. Pharmacol. Exp. Ther.* **319**, 237 (2006).
8. Y. Liu *et al.*, *Cell* **70**, 539 (1992).
9. G. Chen, D. J. Yee, N. G. Gubernator, D. Sames, *J. Am. Chem. Soc.* **127**, 4544 (2005).
10. Materials and methods are available as supporting material on *Science* Online.
11. D. Sulzer, S. Rayport, *Neuron* **5**, 797 (1990).
12. J. A. Steyer, H. Horstmann, W. Almers, *Nature* **388**, 474 (1997).
13. K. Sawamoto *et al.*, *Proc. Natl. Acad. Sci. U.S.A.* **98**, 6423 (2001).
14. T. F. Oo, R. Siman, R. E. Burke, *Exp. Neurol.* **175**, 1 (2002).
15. D. Sulzer, M. S. Sonders, N. W. Poulsen, A. Galli, *Prog. Neurobiol.* **75**, 406 (2005).
16. Y. Schmitz, C. J. Lee, C. Schmauss, F. Gonon, D. Sulzer, *J. Neurosci.* **21**, 5916 (2001).
17. R. G. Staal, E. V. Mosharov, D. Sulzer, *Nat. Neurosci.* **7**, 341 (2004).
18. N. A. Hessler, A. M. Shirke, R. Malinow, *Nature* **366**, 569 (1993).
19. C. Rosenmund, J. D. Clements, G. L. Westbrook, *Science* **262**, 754 (1993).
20. Y. Schmitz, C. Schmauss, D. Sulzer, *J. Neurosci.* **15**, 8002 (2002).
21. M. E. Rice, S. J. Cragg, *Nat. Neurosci.* **7**, 583 (2004).
22. H. Zhang, D. Sulzer, *Nat. Neurosci.* **7**, 581 (2004).
23. N. S. Bamford *et al.*, *Neuron* **42**, 653 (2004).
24. R. M. Wightman *et al.*, *Eur. J. Neurosci.* **26**, 2046 (2007).

25. We thank R. Burke for 6-OHDA injections and advice, M. Sonders for discussion, M. Siu for imaging analysis programming, and J. Schmoranzer for technical support with the TIRFM setup. Columbia University has applied for a patent on fluorescent false neurotransmitters. D. Sames thanks The G. Harold and Leila Y. Mathers Charitable Foundation and Columbia University's Research Initiatives in Science and Engineering. D. Sulzer thanks the National Institute on Drug Abuse (NIDA), the National Institute of Mental Health (NIMH), and the Picower and Parkinson's Disease Foundations. H.Z. thanks the National Alliance for Research on Schizophrenia and Depression. R.H.E. thanks the Michael J. Fox Foundation, the National Parkinson Foundation, NIDA, and NIMH.

Supporting Online Material

www.sciencemag.org/cgi/content/full/1172278/DC1
Materials and Methods
Figs. S1 to S10
Table S1
Movies S1 to S3
References

13 February 2009; accepted 20 April 2009
Published online 7 May 2009;
10.1126/science.1172278
Include this information when citing this paper.

Structure of Rotavirus Outer-Layer Protein VP7 Bound with a Neutralizing Fab

Scott T. Aoki,[1] Ethan C. Settembre,[1]* Shane D. Trask,[1]† Harry B. Greenberg,[2] Stephen C. Harrison,[1,3]‡ Philip R. Dormitzer[1]*‡

Rotavirus outer-layer protein VP7 is a principal target of protective antibodies. Removal of free calcium ions (Ca^{2+}) dissociates VP7 trimers into monomers, releasing VP7 from the virion, and initiates penetration-inducing conformational changes in the other outer-layer protein, VP4. We report the crystal structure at 3.4 angstrom resolution of VP7 bound with the Fab fragment of a neutralizing monoclonal antibody. The Fab binds across the outer surface of the intersubunit contact, which contains two Ca^{2+} sites. Mutations that escape neutralization by other antibodies suggest that the same region bears the epitopes of most neutralizing antibodies. The monovalent Fab is sufficient to neutralize infectivity. We propose that neutralizing antibodies against VP7 act by stabilizing the trimer, thereby inhibiting the uncoating trigger for VP4 rearrangement. A disulfide-linked trimer is a potential subunit immunogen.

Rotaviruses are multilayered, non-enveloped particles with double-stranded RNA (dsRNA) genomes (*1*). Four structural proteins form a complex, three-layered capsid, which packages two viral enzymes and 11 dsRNA genome segments. A double-layered particle (DLP) assembles in the cytoplasm, buds into the endoplasmic reticulum (ER), receives in this process a transient bilayer membrane, and ultimately acquires an outer layer of protein, viral protein 7 (VP7), in place of the transient envelope. VP7 must be present in sufficient quantity and must fold correctly in order to displace the intermediate membrane (*2*–*4*). This unusual maturation pathway results in the coating of a cytoplasmically synthesized and assembled inner particle with an ER-synthesized glycoprotein, but with no intervening membrane in the mature virion.

The surface of the DLP is a $T = 13$ icosahedral lattice of the trimeric protein, VP6, anchored on a $T = 1$ inner layer of VP2 (Fig. 1A). VP7 is likewise a trimer, stabilized by Ca^{2+} ions (*5*). It forms the outermost virion layer, also with $T = 13$ icosahedral packing, by capping the VP6 pillars (*6*–*8*). Assembly of the VP7 shell locks into place a second outer-layer protein, VP4, which is anchored between VP6 pillars and protrudes above the VP7 layer (*9*, *10*). VP4 spikes mediate attachment to cells and undergo a sequence of conformational changes that lead to endosomal membrane penetration (*11*, *12*). Uncoating of VP7, probably by withdrawal of Ca^{2+}, is necessary for these changes to occur (*13*). Thus, VP7 participates both in a membrane-displacing assembly step and in a membrane-disrupting entry step.

Rotavirus infection is the principal cause of severe, dehydrating diarrhea in infants (*14*). Live attenuated vaccines are now being introduced, but the efficacy and practicality of these vaccines in the impoverished settings in which most infant deaths from rotavirus occur have not yet been established (*15*). VP7 and VP4 are the targets of neutralizing and protective antibodies, and the structures and immunogenicities of these proteins underlie ongoing efforts to produce next generation subunit vaccines. Viruses bearing VP7 of at least 15 different serotypes (designated G1 to G15) have been isolated, 11 from humans (*16*, *17*). Epitopes of a number of neutralizing monoclonal antibodies (mAbs) have been determined, but the lack of a three-dimensional structure has precluded systematic study of neutralization mechanisms.

We have determined the crystal structure of the rhesus rotavirus (RRV, serotype G3) VP7 trimer in complex with the Fab fragment of neutralizing mAb 4F8 (*18*). The core of the subunit folds into two compact domains, with disordered N- and

[1]Laboratory of Molecular Medicine, Children's Hospital, Boston, MA 02115, USA. [2]Department of Microbiology and Immunology and Department of Medicine, Stanford University School of Medicine, Stanford, CA 94305, USA, and VA Palo Alto Health Care System, Palo Alto, CA 94304, USA. [3]Howard Hughes Medical Institute, Children's Hospital, Boston, MA 02115, USA.

*Present address: Novartis Vaccines and Diagnostics Inc., 350 Massachusetts Avenue, Cambridge, MA 02139, USA.
†Present address: Laboratory of Infectious Diseases, National Institute of Allergy and Infectious Diseases, Bethesda, MD 20892, USA.
‡To whom correspondence should be addressed. E-mail: harrison@crystal.harvard.edu (S.C.H.); philip.dormitzer@novartis.com (P.R.D.)

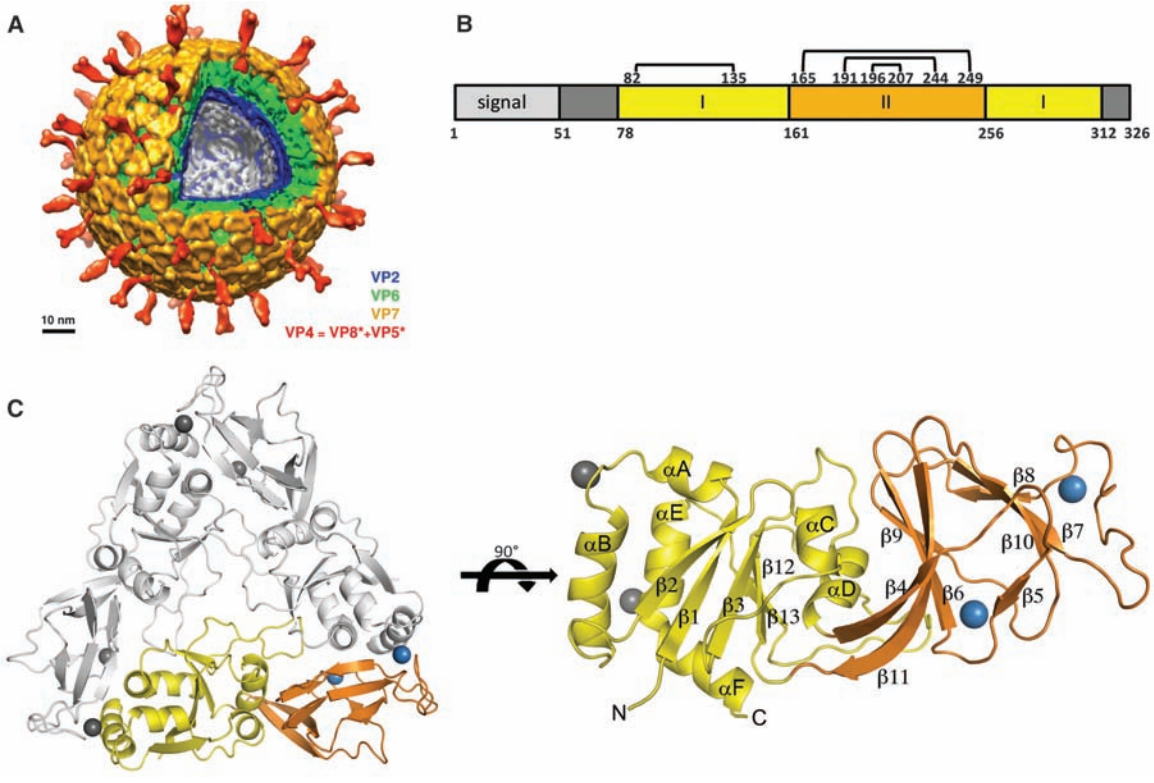

Fig. 1. Structure of RRV VP7. (**A**) Structure of the complete virion as determined by cryo-EM and filtered at 25 Å resolution. The segmentation of the structure is based on reconstructions of the complete virion (*13*) and the VP7-coated DLP (*13*) and on published work of others (*6*–*8*). (**B**) Schematic diagram of the VP7 primary structure, including the signal sequence (residues 1 to 50, light gray). The two domains are in the same colors as in (C); the N- and C-terminal arms, disordered in the crystal structure, are in dark gray. The pattern of intrasubunit disulfide bonds is also shown, with numbers corresponding to the positions of the cysteine residues. (**C**) Ribbon diagram of the trimer (left), viewed along its three-fold axis (i.e., as if looking onto the surface of the virion) with one subunit and one pair of Ca^{2+} ions in color and the other two subunits in gray. The Rossmann-fold domain (domain I) is in yellow, the β-barrel domain (domain II) in orange, and the Ca^{2+} ions in blue. A single subunit, in side view, is shown on the right, with secondary structure elements labeled. See fig. S3 for amino acid sequence of RRV VP7, with secondary structural elements designated.

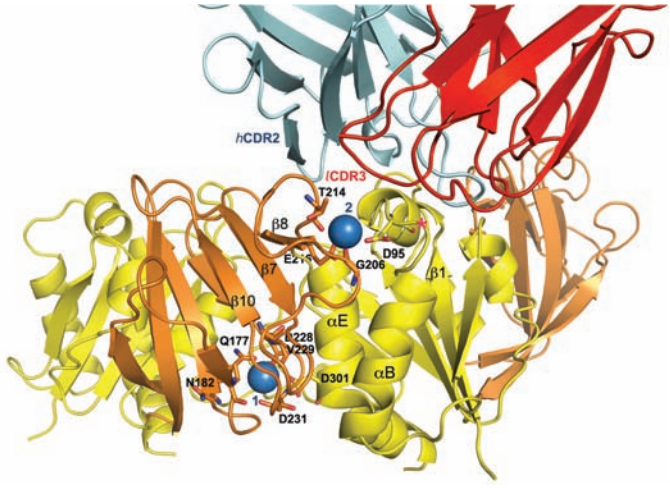

Fig. 2. View of the subunit interface, showing Ca^{2+} ion binding sites (labeled as 1 and 2) and the Fab contact. The view is from a direction that would be 60° around to the right in Fig. 1C, right panel. Residues that contribute to Ca^{2+} ligation (through side-chain groups or main-chain carbonyls) are included in stick representation and labeled. The light chain is in red, the heavy chain in cyan. VP7 colors are as in Fig. 1. The light-chain CDR3, the heavy-chain CDR2, and several secondary-structure elements in VP7 are labeled to provide points of reference and to facilitate comparison with Fig. 1. The heavy-chain CDR3, which like the light-chain CDR3 has extensive contacts with VP7, is the loop in the rear with a projected figure 8–like appearance. The red asterisk on VP7 (at center right) shows the location of the 4F8 escape mutation at position 96. Amino acid abbreviations: D, Asp; E, Glu; G, Gly; N, Asn; Q, Gln; T, Thr; V, Val.

C-terminal arms. There are two Ca^{2+} ions bound at each subunit interface in the trimer. The 4F8 Fab also binds across the trimer interface, apparently stabilizing it even at Ca^{2+} concentrations that would normally lead to dissociation. Known epitopes map either to the same region of the trimer surface or to a region at the interdomain boundary within a subunit. We show that the 4F8 Fab fragment neutralizes infectivity, with a median inhibitory concentration (IC_{50}) only about 30 to 50 times that of the intact, divalent immunoglobulin G (IgG), and we conclude that trimer stabilization, which will block uncoating, is the principal mechanism of neutralization by antibodies that recognize epitopes at the subunit interface. In other work (*13*), we have described a cryoelectron microscopy (cryo-EM) image reconstruction at 4 Å resolution of a DLP recoated with recombinant VP7, showing that the N-terminal arms of a VP7 trimer grip the underlying trimer of VP6. A hinge-bending rearrangement at the VP7 intrasubunit domain interface accompanies DLP binding. The 4F8 epitope at the intersubunit contact remains unaltered.

Recombinant RRV VP7 [expressed in insect cells as described (*5*)] and the Fab fragment of mAb 4F8 form a 1:1 complex that can be isolated by size exclusion chromatography (fig. S1) and crystallized in space group $P4_132$ (a = 244.18 Å, one VP7 subunit plus one Fab fragment per asymmetric unit) from polyethylene glycol (molecular weight 4000) in a pH 5.6 sodium citrate buffer with 0.1 mM $CaCl_2$. Previous efforts to crystallize the VP7 trimer had yielded only very disordered crystals. We recorded diffraction to a minimum Bragg spacing of 3.4 Å resolution, using beamline ID-24C at the Advanced Photon Source, Argonne National Laboratory (table S1). We obtained starting phases by carrying out a molecular replacement search with a library of 244 antibody fragment structures. We performed the rotation function calculations with an integration radius of 35 Å, using the program MOLREP (*19*), with each of the 244 structures as probe. Of these calculations, eight yielded promising solutions, as judged by a distinct difference between the ratio of rotation-function score

to sigma (RF/σ) for the best solution and that for the next best. Inspection showed that the Fab fragments that yielded these solutions all had similar elbow angles and that the positions and orientations of the fragment in the unit cell all had similar values. One of the top solutions was PDB accession number 1DBM, a murine IgG1-κ Fab similar to 4F8. We therefore used this model, modified to display the correct residues of the 4F8 variable domains (sequenced from the hybridoma cell line), for further calculations and model building. Most of the VP7 polypeptide chain was evident in the molecular-replacement electron density, with the exception of N- and C-terminal segments, and we could build a preliminary model without difficulty. The high solvent content (87%) allowed us to calculate a very clear map by solvent flipping (fig. S2), despite the modest resolution (3.4 Å).

The VP7 subunit is a "Rossmann fold" (domain I), with a jelly-roll β sandwich (domain II) inserted between α-helix D and β-strand 12 (Fig. 1, B and C). There are four disulfide bonds, one within domain I and the other three within domain II (Fig. 1B). After initial refinement, a difference map revealed two strong peaks at the subunit interface. Addition of Ca^{2+} ions to the model at each of these positions improved the free *R*-factor. The final model contains residues 78 to 312 (table S1). Asn^{69}, the single glycosylated residue in RRV VP7, is in the disordered, N-terminal arm (fig. S3). Three subunits assemble into a thin triangular plate with a central depression, a variable surface that faces outward on the virion, and a more conserved, somewhat negatively charged, inward-facing surface.

The two Ca^{2+} sites both have side-chain carboxylate and main-chain carbonyl neighbors appropriate for divalent cations, and the contributing side chains are conserved among group A rotaviruses (Fig. 2). There are six protein-derived ligands at site 1 and four at site 2; one or two water molecules, not included because of the limited resolution, presumably complete the coordination sphere at the latter site. Site 2 is close to the Fab interface. The presence of the bound ion might influence the conformation of VP7 loops in contact with the antibody. Mutants in strain RF that confer resistance to low calcium have a Pro^{75} → Leu substitution, sometimes accompanied by a Pro^{279} → Ser mutation (*20*). The former site is in the N-terminal arm, at a location where a leucine might enhance the grip on VP6; the latter, on the inward-facing surface of VP7, is at a point of contact with the outward-facing surface of VP6 (*20*). The resistance to low Ca probably arises from the indirect effect of either mutation in stabilizing the contact with VP6, rather than from a direct effect on the Ca^{2+} sites.

The Fab binds across the intersubunit junction, on the surface of the trimer that will face outward when VP7 coats the virion (*13*) (Fig. 2). The heavy chain carries a majority of the contacts (78% of total buried surface area at the Fab-VP7 interface) to domain I of one subunit and domain II of the other. The one clear light-chain contact is at the site of a neutralization escape mutation (Asn^{96} → Asp) (*21*). Like all well-characterized, VP7-directed neutralizing antibodies, 4F8 binds only trimeric VP7 and not the Ca^{2+}-free monomer (*22*). A number of neutralizing antibodies, including 4F8 and 159, block VP7 uncoating from virions, even in the presence of Ca^{2+} chelators (*22*, *23*). By locking down the subunit interface, these antibodies probably stabilize the trimer, even at very low divalent cation concentrations.

If 4F8 prevents uncoating by stabilizing individual trimers, then the Fab fragment should also neutralize. Figure 3 shows the results of neutralization assays with intact 4F8 mAb and with 4F8 Fab. The IC_{50} for the Fab is about 30 to 50 times that of the intact, bivalent mAb, presumably because of an avidity effect, but the neutralization activity of the Fab is unambiguous. Earlier experiments that came to the opposite conclusion generated the Fab by papain digestion of virion-antibody complexes (*23*, *24*); the concentration of Fab thus produced was probably not sufficient to give a measurable effect.

The sites of mutations in VP7 that permit escape from neutralization by various mAbs map to two regions, 7-1 and 7-2, on the exposed surface of the protein. Each region includes several "epitopes" previously designated by letters (see Fig. 4 and table S2, in which we group the published epitopes into the two structurally defined regions). Region 7-1, which spans the intersubunit boundary, is immunodominant. It contains the positions of escape mutations selected by 58 of 68 tested neutralizing mAbs, including 4F8. Two mAbs select escape mutations in both regions 7-1 and 7-2 (table S2). Modification at position 211 by an oligosaccharide, which would block antibody binding to region 7-1, confers resistance to neutralization by hyperimmune anti-rotavirus serum (*21*). Most or all of the antibodies that bind region 7-1 probably neutralize by a mechanism similar to that proposed above for 4F8. Region 7-2 is at the interdomain boundary within a single VP7 subunit. Antibodies that bind region 7-2 may neutralize by a different mechanism. Analysis of a high-resolution cryo-EM reconstruction of VP7-coated DLPs shows that the subunit undergoes a conformational change when it binds the DLP, with a substantial dislocation at the domain interface but little or no change at the intersubunit contact (*13*). We suggest that antibodies that bind in region 2 stabilize the trimer by fixing the virion-associated conformation, by cross-linking subunits within a trimer, or by cross-linking adjacent trimers on the surface of the virus particle.

The sequences of amino acid residues at positions 87 to 101 and 208 to 211 are conserved among strains within a G serotype but not across different serotypes. These sequences are "signatures" that can be used to predict the serotype of a new isolate (*25*). They correspond to surface ridges on either side of the subunit interface, in regions 7-1a and 7-1b, respectively. Because both homotypically and heterotypically neutralizing mAbs select mutations in region 7-1 (and also in region 7-2), some aspect of antibody binding other than epitope location must determine the breadth of neutralizing capacity (*21*, *26*, *27*).

Regions 7-1 and 7-2 together cover much of the outward-facing surface of VP7. Analysis of

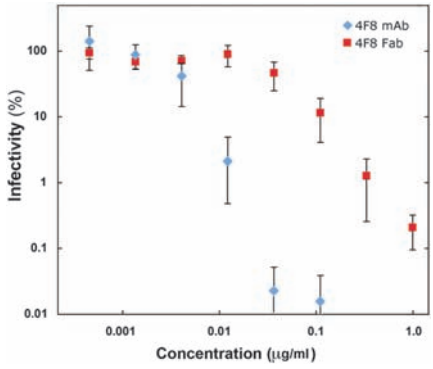

Fig. 3. Neutralization of RRV by the IgG and Fab of mAb 4F8. Percent infectivity is plotted (on a log scale) against antibody or Fab concentration (also on a log scale). Error bars calculated (SDs) are from three independent measurements. See supporting online material for details of the assay.

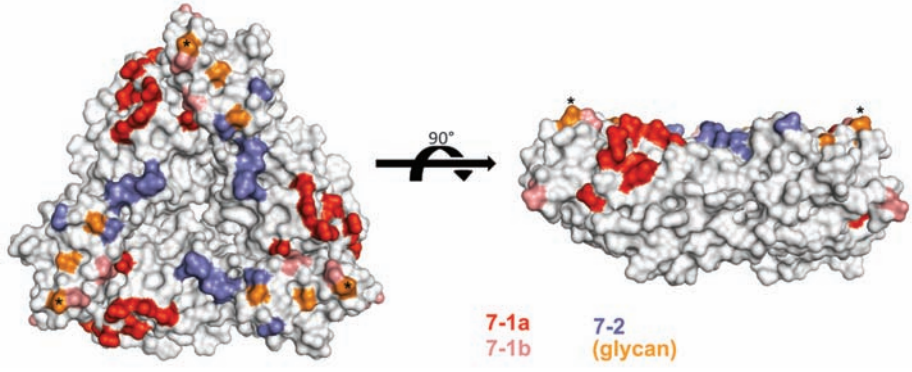

Fig. 4. Positions of neutralization escape mutations selected by various mAbs. The residues cluster roughly into two regions designated 7-1 and 7-2 (see text). Region 7-1 spans the intersubunit boundary; we have divided it into 7-1a (red), on one side of the interface, and 7-1b (pink), on the other. Residues in 7-2 are in blue. The 4F8 Fab (and, by inference, the Fabs of most mAbs that recognize residues in region 7-1) has contacts in both 7-1a and 7-1b (see Fig. 2). Positions at which escape is through a mutation that produces a new glycosylation site are in orange and lie either in 7-1 or 7-2; an asterisk labels residue 211 (see text).

sequences from all 11 human G serotypes shows that most of the variability is in residues on the outward-facing surface of the VP7 trimer (fig. S4). Because there is no extensive conserved patch on this surface, any potential cellular receptor that binds VP7 on the virion must have a very small binding footprint, or its identity and site of interaction must vary among serotypes or isolates. It has been suggested that VP7 may interact with αXβ2 integrins after attachment (*28*). The site proposed as an integrin-binding motif (GPR, resides 253 to 255) is on the inward-facing surface of the trimer and would only be available to interact with integrins after uncoating.

We have designed a disulfide-linked variant of the VP7 trimer by substituting cysteines for Thr^{276} and Gln^{305}, which face each other across the subunit contact. The resulting disulfide is largely buried at the interface. The secreted product of insect cell expression is indeed stably trimeric (fig. S5). The arm-grip mode of association with VP6 thus allows the VP7 trimer to bind and to lock VP4 in place, but cross-linking of the core subunits retards dissociation, probably by several orders of magnitude. These observations support the notion that withdrawal of Ca^{2+} is the uncoating trigger in an endosome.

Rotavirus infection and parenteral immunization with virions both induce a strong VP7-specific neutralizing antibody response (*1*). Recombinant VP7 elicits neutralizing antibodies only inefficiently, probably because the free trimer dissociates; the response can be enhanced by adding a C-terminal membrane anchor, which presumably increases trimer stability by immobilizing the subunit in two dimensions on the cell surface (*5*, *29*). The disulfide cross-linked VP7 trimer, which binds neutralizing antibodies such as mAb 159, is a good first candidate for a more effective, stable, structurally engineered subunit immunogen.

References and Notes

1. M. K. Estes, A. Z. Kapikian, in *Fields Virology*, D. M. Knipe, P. M. Howley, Eds. (Lippincott, Williams & Wilkins, Philadelphia, ed. 5, 2007), pp. 1918–1974.
2. L. Svensson, P. R. Dormitzer, C. H. von Bonsdorff, L. Maunula, H. B. Greenberg, *J. Virol.* **68**, 5204 (1994).
3. T. Lopez *et al.*, *J. Virol.* **79**, 184 (2005).
4. F. Michelangeli, F. Liprandi, M. E. Chemello, M. Ciarlet, M. C. Ruiz, *J. Virol.* **69**, 3838 (1995).
5. P. R. Dormitzer, H. B. Greenberg, S. C. Harrison, *Virology* **277**, 420 (2000).
6. B. V. Prasad, G. J. Wang, J. P. Clerx, W. Chiu, *J. Mol. Biol.* **199**, 269 (1988).
7. M. Yeager, K. A. Dryden, N. H. Olson, H. B. Greenberg, T. S. Baker, *J. Cell Biol.* **110**, 2133 (1990).
8. Z. Li, M. L. Baker, W. Jiang, M. K. Estes, B. V. Prasad, *J. Virol.* **83**, 1754 (2009).
9. A. L. Shaw *et al.*, *Cell* **74**, 693 (1993).
10. S. D. Trask, P. R. Dormitzer, *J. Virol.* **80**, 11293 (2006).
11. L. Fiore, H. B. Greenberg, E. R. Mackow, *Virology* **181**, 553 (1991).
12. P. R. Dormitzer, E. B. Nason, B. V. Prasad, S. C. Harrison, *Nature* **430**, 1053 (2004).
13. J. Z. Chen *et al.*, *Proc. Natl. Acad. Sci. U.S.A.* 10.1073/PNAS.0904024106 (2009).
14. U. D. Parashar, C. J. Gibson, J. S. Bresse, R. I. Glass, *Emerg. Infect. Dis.* **12**, 304 (2006).
15. B. Jiang, J. R. Gentsch, R. I. Glass, *Vaccine* **26**, 6754 (2008).
16. N. Santos, Y. Hoshino, *Rev. Med. Virol.* **15**, 29 (2005).
17. N. Santos *et al.*, *J. Clin. Microbiol.* **46**, 462 (2008).
18. R. D. Shaw, P. T. Vo, P. A. Offit, B. S. Coulson, H. B. Greenberg, *Virology* **155**, 434 (1986).
19. A. Vagin, A. Teplyakov, *J. Appl. Crystallogr.* **30**, 1022 (1997).
20. R. Gajardo, P. Vende, D. Poncet, J. Cohen, *J. Virol.* **71**, 2211 (1997).
21. E. R. Mackow *et al.*, *Virology* **165**, 511 (1988).
22. P. R. Dormitzer, G. W. Both, H. B. Greenberg, *Virology* **204**, 391 (1994).
23. J. E. Ludert, M. C. Ruiz, C. Hidalgo, F. Liprandi, *J. Virol.* **76**, 6643 (2002).
24. F. M. Ruggeri, H. B. Greenberg, *J. Virol.* **65**, 2211 (1991).
25. K. Y. Green *et al.*, *J. Virol.* **62**, 1819 (1988).
26. K. Nishikawa *et al.*, *Virology* **171**, 503 (1989).
27. B. S. Coulson, C. Kirkwood, *J. Virol.* **65**, 5968 (1991).
28. K. L. Graham *et al.*, *J. Virol.* **77**, 9969 (2003).
29. M. E. Andrew *et al.*, *J. Virol.* **64**, 4776 (1990).

30. We thank M. Babyonyshev for help with protein preparations, the staff of the Northeastern Collaborative Access Team (Advanced Photon Source, Argonne National Laboratory) for assistance with x-ray data collection, R. Stanfield for the library of Fab structures, and J. Patton for help with sequence variability analysis. Supported by NIH grant CA-13202 (S.C.H.), by a VA Merit Award and NIH grants AI-21362 and DK-56339 (H.B.G.), and by an Ellison Medical Foundation New Investigators in Infectious Diseases Award (P.R.D.). S.C.H. is an Investigator of the Howard Hughes Medical Institute. Atomic coordinates and structure factor amplitudes for the VP7-4F8 Fab complex have been deposited in the Protein Data Bank (www.rcsb.org) with accession code 3FMG.

Supporting Online Material

www.sciencemag.org/cgi/content/full/324/5933/1444/DC1
Materials and Methods
Figs. S1 to S5
Tables S1 and S2
References

5 January 2009; accepted 28 April 2009
10.1126/science.1170481

Extensive Demethylation of Repetitive Elements During Seed Development Underlies Gene Imprinting

Mary Gehring, Kerry L. Bubb, Steven Henikoff*

DNA methylation is an epigenetic mark associated with transposable element silencing and gene imprinting in flowering plants and mammals. In plants, imprinting occurs in the endosperm, which nourishes the embryo during seed development. We have profiled *Arabidopsis* DNA methylation genome-wide in the embryo and endosperm and found that large-scale methylation changes accompany endosperm development and endosperm-specific gene expression. Transposable element fragments are extensively demethylated in the endosperm. We discovered new imprinted genes by the identification of candidates associated with regions of reduced endosperm methylation and preferential expression in endosperm relative to other parts of the plant. These data suggest that imprinting in plants evolved from targeted methylation of transposable element insertions near genic regulatory elements followed by positive selection when the resulting expression change was advantageous.

Cytosine DNA methylation is a stable epigenetic modification that has roles in transposable element silencing and gene imprinting in plant and animals. In plants, gene imprinting occurs in the endosperm during seed development (*1*). At fertilization, one sperm fertilizes the haploid egg cell, which becomes the diploid embryo, and the other sperm fertilizes the diploid central cell, generating the triploid endosperm. In *Arabidopsis*, the 5-methylcytosine DNA glycosylase DEMETER (DME) demethylates maternal alleles of imprinted genes in the central cell before fertilization, thus establishing methylation asymmetry between embryo and endosperm. Similarly, in maize an imprinted gene is less methylated in the central cell than in the egg cell or sperm (*2*). The asymmetry between embryo and endosperm represents an opportunity to characterize DNA methylation in parallel genomes established simultaneously at fertilization within the same seed.

To compare tissue-specific methylation patterns within developing seeds, we dissected embryo and endosperm from torpedo-stage seeds of two *Arabidopsis thaliana* accessions, Col-*gl* and L*er* (fig. S1A) (*3*). Methylated DNA was immunoprecipitated with an antibody to 5-methylcytosine, sequenced with Illumina Genome Analyzer technology (Illumina, San Diego, CA), and aligned to the reference Col-0 genome. We created methylation profiles using high-quality reads that mapped to only one position in the genome (table S1). Embryo and endosperm methylation profiles were highly correlated (Pearson's $R = 0.91$ for Col-*gl* and 0.89 for L*er*) and share similar features with other whole-

Howard Hughes Medical Institute (HHMI), Fred Hutchinson Cancer Research Center (FHCRC), 1100 Fairview Avenue North, Seattle, WA 98109, USA.

*To whom correspondence should be addressed. E-mail: steveh@fhcrc.org